We are IntechOpen,
the world's leading publisher of
Open Access books
Built by scientists, for scientists

6,900
Open access books available

185,000
International authors and editors

200M
Downloads

Our authors are among the

154
Countries delivered to

TOP 1%
most cited scientists

12.2%
Contributors from top 500 universities

CLARIVATE ANALYTICS
BOOK CITATION INDEX
INDEXED

WEB OF SCIENCE™

Selection of our books indexed in the Book Citation Index
in Web of Science™ Core Collection (BKCI)

Interested in publishing with us?
Contact book.department@intechopen.com

Numbers displayed above are based on latest data collected.
For more information visit www.intechopen.com

GPS Scintillations and Total Electron Content Climatology in the Southern American Sector

Emília Correia,
Marcio Tadeu de Assis Honorato Muella,
Lucilla Alfonsi, Fabricio dos Santos Prol and
Paulo de Oliveira Camargo

Additional information is available at the end of the chapter

Abstract

The radio communication and navigation systems can be strongly affected by the ionospheric conditions, which are controlled by solar phenomena associated with radiation variations and solar wind disturbances. These phenomena can generate ionospheric large-scale plasma redistribution and irregularities with scale sizes varying from centimeters to hundred kilometers. These ionospheric irregularities can produce rapid fluctuations in the amplitude and phase of global navigation satellite system (GNSS) signals, degrading the accuracy of GNSS measurements. Here we give a short review of the ionospheric variations associated with solar phenomena, and the actual state of art in the investigations of long-term (seasonal and solar cycle scales) TEC variations and climatology of scintillations, with focus on the southern American sector. It also presented a new TEC calibration procedure when applied to single-frequency PPP.

Keywords: ionospheric irregularities, scintillation, total electron content, climatology, South America, single-frequency PPP

1. Introduction

Nowadays, the global navigation satellite systems (GNSSs) are widely used in many human activities, particularly for geodetic positioning and navigation, as well for atmospheric monitoring in scientific research. The GNSS systems have been used to obtain the ionospheric total electron content (TEC) often in near real-time and in global scale because the networks ground-based receivers cover large geographic areas. In the last decades, TEC information has given a

great advance in the understanding of the ionospheric structuring and improving our forecasting capacity, which has revolutionized the ionospheric studies. Particularly, the behavior of the ionosphere during geomagnetic disturbed periods has been extensively investigated, showing that F-region response to geomagnetic storms is very complex in space and time, but a general morphology and physical processes have been defined (e.g., [1–13]; and references therein).

The ionospheric knowledge has been used to improve the GNSS positional accuracy, which can be strongly degraded under severe atmospheric disturbances because they can suddenly change the satellite geometry that is essential for geodetic position, in particular for kinematic precise point position (PPP), and are a limiting factor to achieve centimeter accuracy (e.g., [14–16]). The main atmospheric disturbances that affect the GNSS quality signals are the ionospheric steep density gradients, signatures of irregularities of the electron density distribution. Special attention has been given to the ionospheric irregularities investigation, which can vary on a wide range of scale sizes, from centimeters to hundreds of kilometers. The formation and the temporal/spatial evolution of these irregularities affect the propagation of radio signals, causing cycle slips and loss of lock on GNSS receivers and degrading the performance of radio communication and navigation systems [17, 18]. At L-band, amplitude scintillations are due to irregularities with a scale size from hundreds of meters down to tens of meters (according to Fresnel's filtering mechanism), while phase scintillations are caused by structures from a few hundred meters to several kilometers (see, e.g., [18]). In addition, in your way down to the ground, the radio signals could interfere with itself due small changes in their way along the scattered ray paths, resulting in a sort of "space multipath" [19]. The overall of these atmospheric influences can produce rapid fluctuations in the amplitude and phase of GNSS signals, which are known as ionospheric scintillations.

The investigation of scintillations has shown that their activity is stronger at latitudes within the equatorial ionization anomaly (EIA), particularly during post-sunset hours when plasma bubbles are formed in the equatorial F-region driven by the Rayleigh-Taylor instability [20, 21]. Recently, the formation of ionospheric irregularities and plasma bubbles at equatorial region also have shown that they can be driven by gravity waves [22, 23]. The scintillations have been extensively studied at different longitudinal sectors and latitudes, showing a strong dependence on magnetic local time, season, magnetic activity, solar cycle, and geographic location (e.g., [6, 8–13, 19, 24–36]; and references therein).

This chapter provides the characterization of ionospheric scintillations observed with GNSS networks in the South American sector (e.g., [34, 35, 37–40]). The chapter is organized as follows: Section 2 presents the ionospheric variability, Section 3 presents the ionospheric scintillation indices and climatology in South American sector, Section 4 presents the impact of scintillations in a new method for high accurate single frequency precise point positioning (PPP), and finally a discussion section.

2. Ionospheric variability

The solar heating throughout the atmosphere causes large-scale variations associated with diurnal and semidiurnal tides in the thermosphere [41], while the extreme ultraviolet radiation

(EUV) forms the ionosphere. The physical processes in the thermosphere are primarily driven by solar and magnetic disturbances [42], which influence the ionospheric production and recombination, as well transport and frictional heating. The ionospheric conditions have been studied for decades, and particularly there is a good understanding of F-region conditions associated with seasonal, solar cycle, and level of magnetic activity variations. Despite that the predictive capability of its condition is still very poor because the variations appear over a wide range of timescales going from minutes to several days and also depend on the magnetic local time and geographic location. Even during quiet times, that is, under undisturbed geomagnetic conditions, significant ionospheric variability is observed. The low latitude ionosphere is controlled by electrodynamic plasma ($\mathbf{E} \times \mathbf{B}$) drifts driven by thermospheric neutral winds (e.g., [43–45]). The zonal electric fields drive strong daytime E-region eastward currents in the equatorial region, which form two narrow latitudinal bands centered at the dip equator that are called equatorial electrojet (e.g., [46]). The zonal electric fields drive equatorial E and F region vertical plasma drifts (e.g., [47]) that lift the ionospheric plasma at the dip equator, which goes down following the magnetic field lines leading density enhancements located at ~±10–$20°$ from the magnetic equator. The overall process, the plasma lifting followed by their diffusion along the geomagnetic field lines and the formation of the two density maxima away from the equator, is called "fountain effect," and the denser regions are called the crests of the equatorial ionospheric (or ionization) anomaly (EIA) [48]. The thermospheric winds are highly variable because they are driven by changes in the global tidal forcing, and effects of irregular winds, planetary and gravity waves. The planetary waves and tides have been identified as relevant factors affecting the electrodynamics of the lower thermosphere (e.g., [49–55]).

The ionospheric F-region often becomes turbulent and develops electron density irregularities during post-sunset hours [56]. During the day, the electrical field is eastward and it reverses to the west after sunset, but during sunset an enhanced eastward electric field develops, the so-called pre-reversal enhancement (PRE) [44, 57, 58]. The PRE drives an upward vertical plasma drift at magnetic equatorial region, and the bottom of the F-region becomes unstable to the Rayleigh-Taylor instability [59], developing large-scale plasma depletions (plasma bubbles). These bubbles ascend upwards over the magnetic equator, causing a redistribution of ionization similar to the fountain effect. The latitudinal extension of the plasma bubbles is defined by the upper height limit they reach in their rise up above the magnetic equator [60] and can intersect the crests of the EIA, where the steeper density gradients on the edges of the plasma bubbles favor the generation of smaller scale irregularities [56, 61, 62]. The plasma bubbles practically disappear after local midnight and are most intense during the equinoctial months and during the solar maximum years [63, 64]. These conditions favor the scintillations to occur most frequent and severe around the EIA crests, in particular after sunset due to the generation of irregularities caused by the intersection of the plasma bubbles with the regions of larger background electron density.

The ionosphere can be strongly disturbed during geomagnetic storm-time periods. These storms are terrestrial magnetospheric perturbations caused by the impact of interplanetary coronal mass ejections (ICMEs), and corotating interaction regions associated with high-speed streams (HSS), which are the most geo-effective solar wind phenomena. The coupling process involving the solar wind, the interplanetary magnetic field (IMF) and the magnetosphere strongly affects the high latitude ionospheric electrodynamics. The magnetosphere compression during geomagnetic

storms induces intense electric fields and increases its convection. During these processes, the interplanetary electric field (IEF) is mapped along the magnetic field lines to the high latitude ionosphere, but can also propagate across them and promptly appears in the low latitude ionosphere, when it is called of prompt penetration electric field (PPEF). The effect of PPEF at the equatorial ionosphere has been observed during the first hours of the main phase of geomagnetic storms, suggesting a long-duration penetration of interplanetary electric field to the low-latitude ionosphere without shielding (e.g., [5, 65–68]). The equatorial ionosphere under the effect of the PPEFs is convected upward in the dayside and downward in the night side [66]. The PPEFs are stronger than the fields associated with the normal fountain effect resulting in a higher elevation of the equatorial plasma [5], and consequently the crests of the EIA departs more from magnetic equator and can reach middle latitudes (~±20–30°). At high latitudes, the precipitation of energetic particles enhances ionospheric conductivities and generates intense electrical currents in the auroral zone [3]. The dissipation of these currents by the Joule effect heats the local plasma that expands, changing the lower thermospheric composition and driving large-scale neutral winds [3, 4, 42]. Thus, major geomagnetic storms results in a large-scale ionospheric thermal plasma redistribution involving all latitudes from the equatorial through the polar region. Particularly F2-region shows very complicated spatial and temporal behavior (e.g., [9]), but a general morphology and physical processes have been established (e.g., [1–4, 7, 9]). F2-region variations during geomagnetic disturbed periods are called ionospheric storms and are detected as an increase (positive) or depletion (negative) of electron density associated with electrodynamics processes or neutral composition changes (e.g., [4]), respectively. Their morphology is a function of the amount of energy inputted in the high latitude during the main phase of geomagnetic storm [69], as well of the station latitude and longitude, local time of storm onset, storm time and season.

3. Ionospheric scintillations

3.1. Scintillation indices

Scintillations are rapid fluctuations in the amplitude and phase of GNSS signals produced by the ionospheric irregularities, which are responsible by the refraction and diffraction of trans-ionospheric signals [20, 70].

The ionospheric scintillations are evaluated from 60 s amplitude (S4) and phase scintillation (Phi60) indices, which give information about intermediate (around hundreds of meters) and large (above hundreds of meters)-scale size irregularities, respectively. The scintillation indices are obtained by using GNSS dual-frequency receivers recording data at a high data sampling rate of 50 Hz, which also compute the total electron content values.

The S4 index can be interpreted as the standard deviation of the received power (C/NO) normalized by its mean value and the Phi60 index is the standard deviation (in radians) of the carrier phase computed over 60 s time interval. The indices are obtained as Eqs. (1) and (2) [71].

$$S4 = \sqrt{\frac{<I^2> - <I>^2}{<I>^2}}, \tag{1}$$

$$Phi60 = \sqrt{<\varnothing^2> - <\varnothing>^2}, \tag{2}$$

Class	Index value
Weak	$0.1 < S4 < 0.25$ or $0.1 < Phi60 < 0.25$
Moderate	$0.25 < S4 < 0.7$ or $0.25 < Phi60 < 0.7$
Strong	$S4 > 0.7$ or $Phi60 > 0.7$

Table 1. Classification of the ionospheric scintillation severity.

where $\diamondsuit$ denotes 60 s average, I is the signal intensity and $\varnothing$ the signal phase at GPS L1 frequency (1.575 GHz) sampled at 20 ms (50 Hz).

The S4 and Phi60 indices are used to classify ionospheric scintillation severity, which can be separated in three categories: strong, moderate and weak scintillations, for example, as shown in **Table 1**.

3.2. Ionospheric scintillation climatology in south American sector

The morphology of the Earth magnetic field favors the occurrence of strong scintillations at high latitudes, and intense at equatorial region between about 20°N and 20°S magnetic latitudes [20, 72]. Particularly in the South American sector, the F-region irregularities present peculiarities due to the large longitudinal variation in the magnetic declination angle [38, 73, 74], as well by the influence of the South American Magnetic Anomaly (SAMA). The SAMA is the region on the Earth where the magnetic field has the lowest intensity values, allowing enhancement of energetic particle precipitation into the atmosphere [75]. The enhanced ionization in the SAMA region produced by the particle precipitation is a regular feature, which modifies the quiet ionospheric physical conditions increasing the F-layer vertical drift over the eastern sector as compared to the western sector of South America, which can be drastically modified during magnetospheric disturbances (e.g., [75]; and references therein).

The investigation in the South America sector has been improved in the last decades after using GNSS receivers networks dedicated to monitor ionospheric scintillations. Today, there are three GNSS networks, the GPS Low-Latitude Ionospheric Sensor Network (LISN) that is operating since November 2011 with an array of 45 receivers [76], 15 of them over the Brazilian territory, where they are complimented with one array of 12 GPS Ionospheric Scintillation Monitoring Receivers (ISMR) of the GPS Scintillation Monitors network (SCINTMON) [38] and other with 10 ISMR of the Concept for Ionospheric Scintillation Mitigation for Professional GNSS in Latin America and Countering GNSS high Accuracy applications Limitations due to Ionospheric disturbances in Brazil (CIGALA/CALIBRA) project [77]. At high latitude, these networks are complimented with GPS ionospheric scintillation and total electron content (TEC) monitor receivers (GISTM) that covers a large area from sub-equatorial Latin America to the South Pole [71].

3.2.1. Quiet geomagnetic conditions

Ionospheric irregularities commonly appear in the regions of enhanced or depleted electron density. These regions are associated with the crests of the EIA anomaly located at latitudes ~15–20° from the magnetic equator, where strong scintillations have been observed particularly

during sunset hours. Before GNSS era, Aarons [20] using ionosondes and VHF systems showed the scintillation intensities, produced by smaller scale ionospheric irregularities, were stronger in the EIA crests after sunset hours under the influence of plasma bubbles. A comprehensive study of the occurrence of irregularities over the south EIA crest in Brazil during two decades was reported by Sobral et al. [21], which shows the plasma bubbles occurrence has a broad maximum around summer months (from September to April), with a significant increase from low to high solar activity levels during the equinoctial months of March-April and September-October. De Paula et al. [38], using GPS L1-band receivers in the Brazilian territory, reported the characteristics of small-scale irregularities that produced strong scintillations in the post-sunset equatorial ionosphere from 1997 to 2002, the ascending phase of the solar cycle 23. They reported that the ionospheric irregularities are stronger in the southern crest of the EIA, and present a seasonal variation occurring predominantly from September to March during magnetic quiet periods, being more intense during December (local summer). They also show a large longitudinal variation in the South American sector showing that the irregularities are most intense in the EIA crest in Brazilian sector than over Argentinean sector, which is attributed to the large longitudinal variation of magnetic declination in this sector. During quiet magnetic periods, the irregularities occur in the sunset-midnight local time sector while during magnetic storms their occurrence can extend to the midnight-sunrise sector. Akala et al. [39] using a chain of GPS receivers along the western longitude sector of South America, during different levels of solar activity, also shows the scintillations occur predominantly at post-sunset hours and decay before or around local midnight, with stronger activity and longer durations in the months of March and January, which means in the March Equinox and December solstice; and in particular the station near northern crest of the EIA recorded the highest occurrences of scintillation especially during periods of high solar activity.

Spogli et al. [24], using GISTM receivers located between South America, South Atlantic Ocean and Antarctica, defined crucial areas in the ionosphere where the probability of scintillation occurrences is higher. These areas were called ionospheric scintillation "hot-spots" and were defined using a climatological representation given by the Ground Based Scintillation Climatology (GBSC) technique [19]. They showed that there are two main hot-spots over South America, first one associated with the post-sunset (POST) hours at low latitudes located in the magnetic latitude (MLAT) range 15–25°S and magnetic local time (MLT) between 20 and 24 h, and another one associated with particle precipitation region (SAMA) nearby SAMA region located in the MLAT range 22–24°S and MLT between 0 and 24 h. At high latitudes, they identified three scintillation hot spots, one associated with particle precipitation region in the polar cusp (CUSP, MLAT: 74–82°S and MLT: 10–14 h), other associated with place where the irregularities are induced by reconnection from the magnetotail (MLAT: 68–82°S, MLT: 20–4 h), and other one associated with polar cap patches (PATC, MLAT: 82–90°S, MLT: 0–24 h). The POST hot spot shows scintillation intensifications in March and November, in agreement with the intensification of pre-reversal at equinoxes (e.g., [78]). The hot-spot intensification is stronger in November probably due to the superposition effects associated with the spring equinox and the local summer. The SAMA hot spot also shows one stronger enhancement in November similarly the observed at POST hot spot. They also confirm that in the Brazilian longitudes, the irregularities are more intense in the September (spring) equinox

and summer months [38]. At high latitude the two main hot spots identified as CUSP and PATC show enhancements at equinoxes that are attributed to direct particle precipitation.

Muella et al. [34] investigated the scintillation occurrence from 2002 to 2006, during the descending phase of the 23rd solar cycle, at two sites located in the inner regions of the northern and southern crests of the equatorial ionization anomaly in the Brazilian sector. They showed that the scintillation occurrences during sunset hours present a north-south asymmetry, being ~10% higher over the southern EIA crest than over northern one during solar maximum. This asymmetry was considered to be a possible influence of the SAMA on the scintillation activity. The scintillation occurrence also showed a broad minimum in June and maximum in December over both crests. On a recent investigation of scintillation occurrence at Cachoeira Paulista near the south EIA crest, covering almost the two last solar cycles (1998–2014), Muella et al. [37] showed that the maximum occurrence of scintillations observed during the peak of 23rd solar cycle was 20% higher than that one observed for the 24th, which was the weakest cycle in the last century. This behavior can be attributed to the scintillation intensity dependence on the electron density gradients and the thickness of irregularity layer, which are driven by the intensity of the solar extreme ultraviolet radiation (EUV). In addition, the fewer occurrences of scintillation in the maximum of the 24th solar cycle at Cachoeira Paulista could also be associated with the secular variation in the dip latitude, which changed ~3° in south direction from 1997 to 2014.These results on the long-term trend analysis and climatology of scintillations at the EIA region are shown in **Figure 1**. The colored contours in the upper panel of **Figure 1** show the nocturnal occurrence statistics of scintillation from 1998 to 2014 for $S_4 > 0.2$ as function of universal time (UT = LT + 3 h) and the mean F10.7 cm solar flux index. For the type of the GPS receiver used to measure scintillations, the threshold of $S_4 > 0.2$ can be considered above the level of multipath and noise effects, which may produce very weak scintillations ($S_4 < 0.2$). The middle panel shows the occurrence for the strongest levels of scintillations (threshold of $S_4 > 0.5$), whereas the color scale bar indicates the percentage of occurrence used in the plots of scintillation statistics. The monthly mean variation of the F10.7 cm solar flux is shown in the lower panel and depicts its changes from the ascending phase of solar cycle 23rd to the maximum of solar cycle 24th. **Figure 1** reveals that the patches of larger occurrence of scintillations are observed from 23:00 to 04:00 UT between the months of September and March and mainly around the solar maximum years.

The climatology of the onset time of ionospheric scintillations near the southern crest of EIA over Brazilian territory, covering a period between solar cycles 23 and 24, showed that their start time is about 40 min earlier in the months of November and December when compared to January and February, suggesting an association with the ionospheric pre-reversal vertical drift (PRVD) magnitude and time [79].

An investigation of the equatorial scintillations over São Luis (2.33°S, 44.21°W, dip latitude 1.3°S) was done by Muella et al. [35] during different solar activity levels of the 23rd solar cycle (1999–2006). The study showed the scintillations occurred more frequently during the years of high solar activity, but strong scintillation variability was also observed during the descending phase of the solar cycle. The scintillations occurred predominantly during pre-midnight hours with a broad maximum in the summer. They observed a weak level of scintillations all
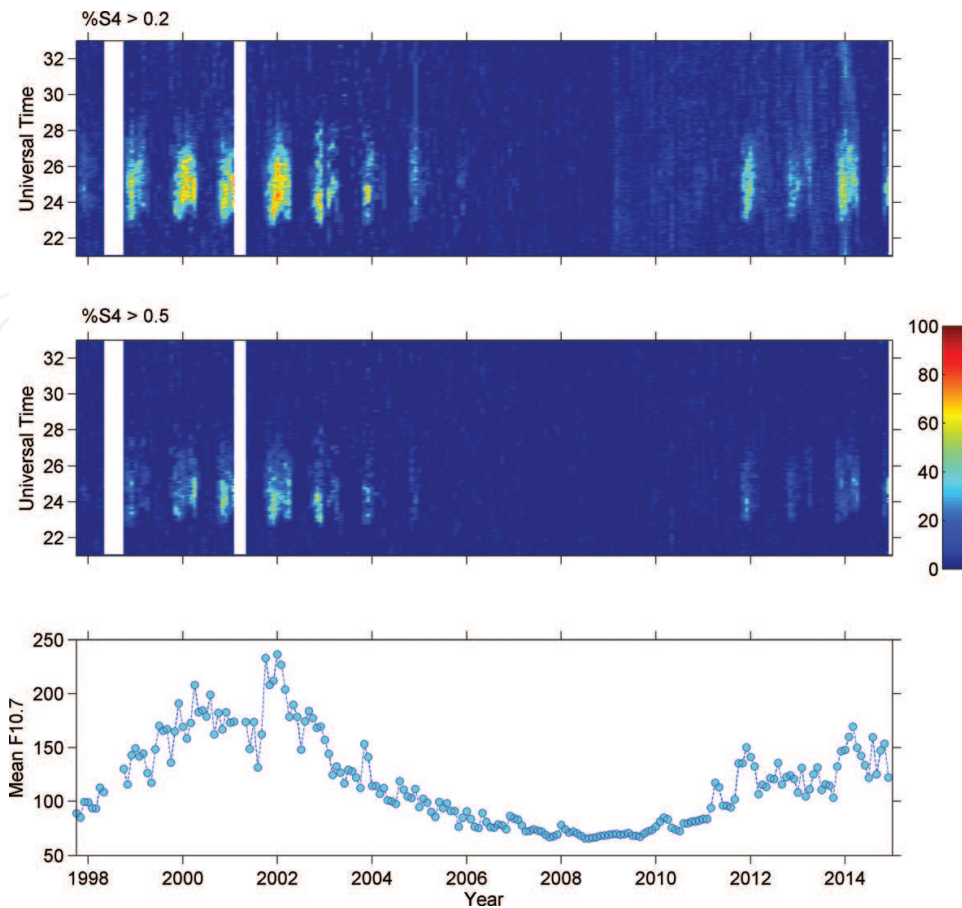
Figure 1. Occurrence climatology of the GPS L1-frequency scintillation (1998–2014) at Cachoeira Paulista for two threshold levels of the S_4 amplitude scintillation index as function of universal time (UT = LT + 3 h) and the mean solar radio flux in 10.7 cm (F10.7 index). The upper and middle panels denote the nocturnal occurrence climatology for the levels of $S_4 > 0.2$ and $S_4 > 0.5$, respectively. The colored bar indicates the percentage of scintillation occurrence used in the plots. The monthly mean variation of the F10.7 cm solar flux is shown in the bottom panel to depict the changes in the solar cycles. [after Muella et al. [37]. Reproduced with permission of the Copernicus publications on behalf of the European geoscience union].

over the year, however, during the winter months near the years of solar maximum, some stronger levels of scintillations were observed at comparable rate with the weak scintillations.

The ionospheric scintillations are driven by zonal drift of the irregularities, so the investigation of the spatial and temporal variations of the irregularities have been done in the last decades. The study of the zonal drift driven scintillations in the South American sector has shown that: a latitudinal gradient in the irregularity zonal velocities is associated with the vertical shear of the zonal drift in the topside equatorial ionosphere [80]; at two magnetic conjugate sites over Brazilian territory, the magnitude of the zonal velocities in the site inside the SAMA region was ~12% larger than in the conjugate one [81]; during nighttime, there is a strong correlation between neutral winds and scintillation drifts near magnetic equator [82]; the irregularity of the zonal drifts shows a negative gradient with increasing geomagnetic latitude [83]; and that the magnitude of the zonal velocities might be reduced at the inner regions of the EIA due to the latitudinal variation in the ion drag force [35]. The nighttime zonal drift velocities of the ionospheric irregularities increase in association with increasing EUV solar radiation [37, 84, 85],

which can be produced by the fact that in years of higher solar activity, the thermospheric zonal wind velocities are higher enhancing the solar thermal tide [86].

3.2.2. Disturbed geomagnetic conditions

The ionospheric electrodynamics conditions depend on magnetosphere-ionosphere-thermosphere system, which can be strongly disturbed during geomagnetic storms. During geomagnetic storms, the magnetosphere is compressed inducing intense electric fields and increasing the magnetospheric convection. The strongest geomagnetic storms are mainly produced by the impact of solar wind disturbances associated with geoeffective solar coronal mass ejections (CMEs) and coronal hole solar high speed streams (HSS) on the magnetosphere, which results in a highly inhomogeneous ionosphere, producing steep electron density gradients and irregularities. The ionospheric electron density distribution changes as a function of the solar wind input energy in the high latitude upper atmosphere, which occurs during the main phase of the geomagnetic storms [69].

The spatial and temporal variations of F2-region during geomagnetic storms are called ionospheric storms, and their morphology depends on the site location, local time of geomagnetic storm onset, storm time and season. Despite the very complex ionospheric behavior during disturbed periods, there is a general understanding about its morphology and physical processes (e.g., [1–4, 7, 9]). The negative phase of ionospheric storm is attributed to changes in the thermosphere at middle and high latitudes due to the heating in the auroral zone, mainly by Joule dissipation [87], occurring at all seasons but in winter. In contrast, the positive phase occurs at middle and low latitudes mainly in winter season and involves more complex physical processes associated with uplifting due vertical drift, plasma fluxes from the plasma sphere, and downwelling produced by storm-induced thermosphere circulation at low latitudes (e.g., [3, 7, 9]). The vertical drift during daytime is controlled by equatorward winds at middle latitudes during the winter, and at equatorial region is driven by the EIA anomaly in association with prompt penetration electric field effect (PPEF) [5], resulting in an enhancement of the electron concentration because the photoionization is still operating (e.g., [3, 88]).

At middle latitudes, TEC enhancements are observed during the main phase of geomagnetic storms in the dusk sector, which are called storm-enhanced density (SED), and have been associated with large-scale redistribution of ionospheric plasma, covering a large extension from equatorial to polar region [89]. This phenomenon has been observed during the first hours of the main phase storm when the fountain effect at the equatorial region is reinforced by the PPEF, moving EIA crests from low to middle latitudes. The middle latitude EIA crest at dusk sector, under electrodynamic processes, has its plasma redistributed in longitude and latitude generating plumes of SED [90], which can be transported into dayside cusp where enter the polar cap and form the called tongue of ionization (TOI; [8, 10–13, 24, 89]; and references there in) at polar region. The ionospheric plasma redistribution during geomagnetic storms is a function of their intensity, magnetic local time, storm time, latitude and season.

The ionospheric regions affected by impact of geomagnetic storms show a strong intensification of scintillation occurrence. At high and middle latitudes, these regions are the night side auroral oval due to the particle precipitation events [12, 91, 92], the cusp on the dayside

in association with SED, and the polar cap in association with TOI, while at equatorial latitudes the scintillations are associated with regions under the influence of the EIA anomaly. Similarly, the ionospheric storms, the occurrence of scintillations during geomagnetic disturbed periods also are function of magnetic local time, season, magnetic activity, solar cycle, and geographic location [12, 13, 19, 25, 26]. The ionospheric irregularities can be inhibited during magnetic storms with main phase occurring during daylight hours, but can be intensified during any season when main phase storm coincides with the hours of the pre-reversal electric field is maximum (e.g., [75]). De Paula et al. [38] from an investigation of small scale irregularities (~400 m) at equatorial and low latitudes over Brazilian territory obtained that during geomagnetic storms they can occur at any epoch of the year, present largest intensities in the south EIA crest, could extend from sunset-midnight to midnight-sunrise sector during some storms, are enhanced during PPEF occurring during post sunset hours, and can be suppressed during daytime main phase storm under the disturbance dynamo effect. In association with geomagnetic storms, the large-scale irregularities (few km) have shown a seasonal variability [93]. On the other hand, an investigation of the F-region under the impact of the geomagnetic storm occurred on June 2013, from equatorial to middle latitudes in both hemispheres over American sector, showed that the ionospheric irregularities were observed confined in the equatorial region before and during the storm, which shows this storm did not affect the generation or suppression of irregularities [94].

An investigation of the 26–27 September 2011 moderately intense geomagnetic storm impact in the ionosphere at middle and high latitudes in the South American sector showed that during its dayside main phase two SEDs were observed at middle latitudes [13]. These SEDs were attributed to a combination of processes, including the PPEF effect from low latitudes during a couple of hours just after the storm onset, and dominated by the disturbance dynamo effect from high latitudes during its evolution. The plumes of these SEDs were located near the dayside cusp and result in TOI formations observed in nightside polar cap region. In association with the middle latitude SEDs and polar cap TOIs were observed strong ionospheric scintillations.

4. The impact of ionospheric scintillations in a new single-frequency PPP method

New analysis about the GNSS positioning was performed by Prol et al. [95] in order to evaluate the ionospheric delay retrieved by a new method for TEC calibration when this method was applied to correct the single-frequency PPP. The results revealed the possibility of performing the single-frequency PPP corrected by a TEC calibration and obtaining a similar accuracy to the double-frequency PPP. It suggested that almost all of the first-order ionospheric effect was eliminated by the TEC calibration method. Additionally, the single-frequency PPP corrected by the new method was very sensitive to the impact of the ionospheric scintillations. In fact, the proposed single-frequency PPP appeared to be even more sensitive to ionospheric scintillation in comparison with the single-frequency PPP corrected by traditional ionospheric models and the double-frequency PPP. In order to present the impact of the ionospheric scintillations in the proposed single-frequency PPP, this section describes the developed method for TEC calibration and some experiments and results.

TEC can be expressed as the integral of the electron density n_e along the path between the GNSS satellite (s) and the receiving antenna (r), in a column whose cross sectional is equivalent to 1 m². It can be written as:

$$TEC = \int_r^s n_e \, ds, \tag{3}$$

being the ionospheric delay given by the following relation with TEC:

$$I = \frac{40,3}{f^2} TEC, \tag{4}$$

where I represents the ionospheric delay and f the signal frequency.

The ionospheric delay is related to the GNSS observations by the following equation for the code:

$$P_L = \rho + c(d\,t_r - d\,t^s) + I_L + T + d\,m_L + \epsilon_P, \tag{5}$$

and the following equation for the carrier phase:

$$\lambda_L \phi_L = \rho + c(d\,t_r - d\,t^s) - I_L + T + d\,m_L + \lambda_L N_L + \epsilon_\phi, \tag{6}$$

where the frequency-dependent terms are referred by L, ρ is the geometric distance, c is the speed of the light in vacuum, $d\,t_r$ and $d\,t^s$ are the receiver and satellite clock errors, T refers to the tropospheric delay, dm is the multipath, N_L is an ambiguity term, λ is the wavelength and ϵ represents the noise in code (P) and phase (ϕ).

The method to estimate TEC (Eq. (3)) using GNSS observations (Eqs. (5) and (6)), is performed in three steps. In the first step, a phase leveling estimation based on the code information provides the ambiguity terms. In this regard, the difference between ambiguities (ΔN) of two GPS frequencies (L1 and L2) in a unique arc of data is calculated through:

$$\Delta N = (\lambda_1 N_1 - \lambda_2 N_2) = \frac{1}{n_{obs}} \sum_{j=1}^{n_{obs}} \left[(P_{2j} - P_{1j}) - (\lambda_1 \phi_{1j} - \lambda_2 \phi_{2j}) \right], \tag{7}$$

where only arcs with a minimum of 5 min of continuous data are used. Once the ΔN term is obtained for all arcs of a specific day, the receiver DCB (Differential Code Bias - Δb_r) is obtained by the daily weighted mean of the phase difference ($\lambda_1 \phi_{1j} - \lambda_2 \phi_{2j}$), the initial TEC, the leveling ambiguity and the satellite DCB (Δb_s). The receiver DCB is derived by the following weighted mean:

$$c\Delta b_r = \frac{1}{\sum_{i=1}^{n_{arc}} \sum_{j=1}^{n_{obs}} w_{ij}} \sum_{i=1}^{n_{arc}} \sum_{j=1}^{n_{obs}} w_{ij} \left[(\lambda_1 \phi_{1j} - \lambda_2 \phi_{2j}) - \frac{TEC_{ij}^{gim}}{F} - \Delta N - \Delta b_{si} \right], \tag{8}$$

with

$$F = \frac{f_1^2 f_2^2}{40.3(f_1^2 - f_2^2)} \text{ and } w_{ij} = \frac{1}{(\sigma TEC_{ij}^{gim}/F)^2}, \tag{9}$$

being σTEC_{ij}^{gim} the standard deviation of the initial TEC, which is derived from the Global Ionospheric Maps (GIMs) of the International GNSS Service (IGS) and their root-mean-square (RMS) maps. In addition, the satellite DCB Δb_{si} is obtained from GIMs. Therefore, as the satellite DCB and the initial TEC are obtained from GIMs, it is expected that the estimated receiver DCB is related to the DCB referential frame defined by IGS.

Once the ambiguity leveling (first step) and the receiver DCB estimation (second step) are done, the third step consists in the TEC estimation. TEC is directly calculated along the path of the GNSS signal with the following equation:

$$TEC = F\left[(\lambda_1 \phi_1 - \lambda_2 \phi_2) - \Delta N - c(\Delta b_s + \Delta b_r)\right], \qquad (10)$$

where the TEC is derived for each GNSS observation, that is, TEC is estimated with the same time resolution as the phase and code collection rate.

Two close GNSS stations located at Rio de Janeiro in Brazil have been selected to make the experiments. The TEC estimation procedure was performed in the station RIOD (lat. Mag. 36.47° S), and the ionospheric delay correction was applied in the station ONRJ, which is located 12 km away. Using the configuration of short distances apart, it is possible to mitigate the problems of spatial gradients of the ionosphere. In addition, the receivers and antennas are from different brands in order to avoid possible correlations between clock and ambiguities of the stations. In this way, it has been as much as possible to isolate the degradation of the ionospheric scintillations in the PPP results.

Prol et al. [95] evaluated the analysis of the performance of the new TEC calibration procedure when applied to PPP for 120 days with six distinct configurations of base and rover stations, and the TEC performance is assessed by applying the estimated TEC from the base station to correct the ionospheric delay in a nearby rover receiver. Just to show the potentiality of the new procedure, here are shown the results of the analysis for two specific days with and without ionospheric scintillations.

Figure 2 shows an example of the calibrated TEC in RIOD during epochs with and without evidences of ionospheric scintillations. Each colored line represents the slant TEC calculated for a distinct satellite, that is, one colored line refers to the slant TEC of one GPS satellite. The Day Of Year (DOY) 005 of 2013 is shown in the top panel, which refers to the summer solstice in the south crest of EIA. On the other hand, DOY 191 of 2013 is referred to the winter. As it can be seen, the maximum of TEC in the summer solstice reaches around 150 TECU in the slant direction during the daytime. The magnitude of the TEC in daytime is reduced in the winter for up to 100 TECU, mainly due to the reduced intensity of the solar irradiation. However, TEC variability in the daytime is similar. In contrast, the nighttime between 22 and 04 LT presents a significant difference in terms of the TEC variability. The maximum TEC in the nighttime is reduced from 60 TECU in the solstice up to 30 TECU in the winter. Additionally, the high TEC variability evidenced between 22 and 04 LT is associated to the plasma depletions propagating trough the Brazilian region. In fact, the high magnitude of the TEC observations in comparison with the TEC variability makes the impact of the ionospheric
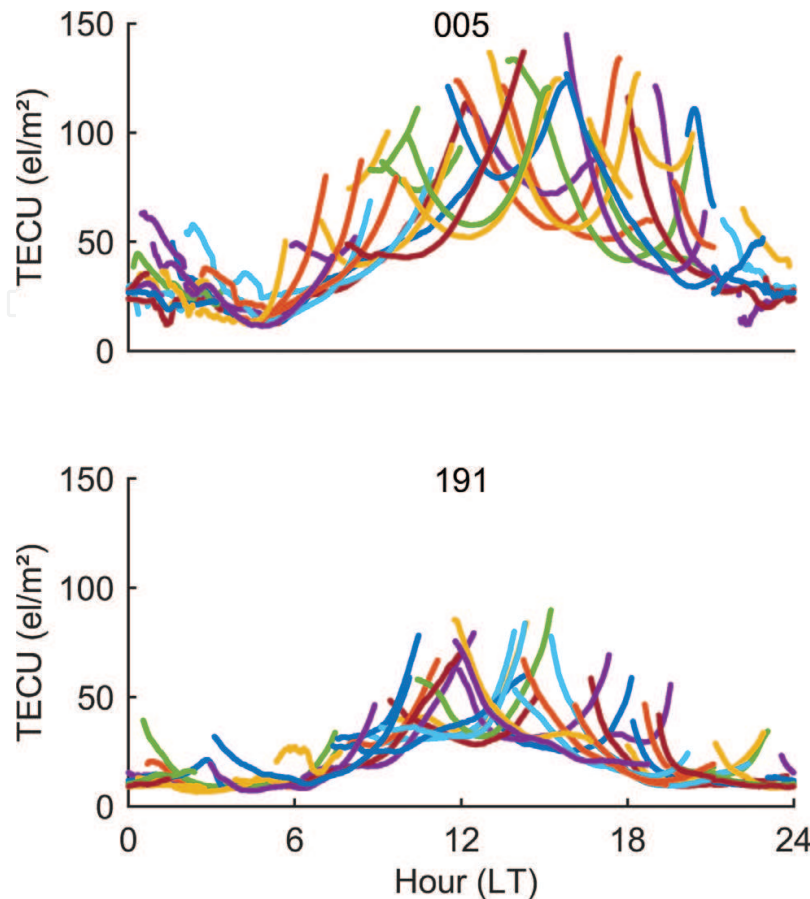
Figure 2. TEC estimation with the proposed procedure at RIOD station on 2013 for DOY 005 during the summer (top panel) and DOY 191 during the winter (bottom panel). Each colored line represents the slant TEC calculated for a distinct GPS satellite.

scintillation not so clearing TEC. However, the impact of the ionospheric scintillations is much more easily seen when looking to the single-frequency PPP performance.

RTKLIB is adapted for the use of the calibrated TEC during the single-frequency PPP. Among the PPP configurations, it is used the kinematic mode, a combined solution obtained by forward and backward filters, a cut-off angle of 10°, Earth tides corrections, the estimation of tropospheric delay during PPP, IGS precise ephemerides, satellite clock corrections with a 30 s rate (clk_30s), global positioning system constellation, correction of the phase center variation of the antenna, phase wind up corrections, no strategy for ambiguity solution and corrections of the differential instrumental bias between the civil and precise codes (C1-P1) when P1 was not available. In general, three modes of PPP are analyzed: (1) using the ion-free observation (PPP/if); (2) using L1 and the ionospheric delay from GIMs from UQRG (UPC Quarter an hour Rapid GIM), identified as PPP/uqrg; and (3) using L1 and the calibrated TEC through the proposed method (PPP/tec). Indeed, the PPP/if solutions are obtained using the ion-free observation of the carrier phase, which means that a linear combination is carried out with the L1 and L2 frequencies to eliminate the first-order effect in the ionospheric delay. In the case of PPP/uqrg, the observation used in the PPP Kalman Filter is related to the L1

frequency but corrected from the ionospheric delay derived from UQRG GIMs. The PPP/tec is similar to PPP/uqrg, but the ionospheric delay is derived directly from Eq. (10). The reference coordinates of ONRJ has been obtained from the Sistema de Referencia Geocéntrico para las Américas (SIRGAS) final solutions at epoch 2013, where a time update was performed to make the coordinates consistent with the PPP solutions.

Figure 3 shows the performance of PPP/if, PPP/tec and PPP/uqrg in terms of the three-dimensional (3D) error of the estimated coordinates. Each point represents the error of the PPP solution calculated in each processing epoch in kinematic mode. Since it was used a combined filter of forward and backward solution, there is no need for time convergence in the solution. Consequently, the remaining errors are related to the terms not efficiently mitigated and, as can be seen, the PPP/tec (blue points) was obtained with a high accuracy in many hours, except to the hours when is typically observed ionospheric scintillations.

In general, the proposed method allowed having the single-frequency PPP with a similar accuracy than the double-frequency PPP. The root mean square error (RMSE) obtained for PPP/if in DOY 191 was 0.04 m with a standard of 0.04 m, the RMSE of PPP/tec was 0.09 m with a standard deviation of 0.04 m and the RMSE of PPP/uqrg was 0.47 m with a standard deviation of 0.65 m. In the case of DOY 005, the RMSE of PPP/if was 0.04 m with a standard of 0.04 m, the RMSE of PPP/tec
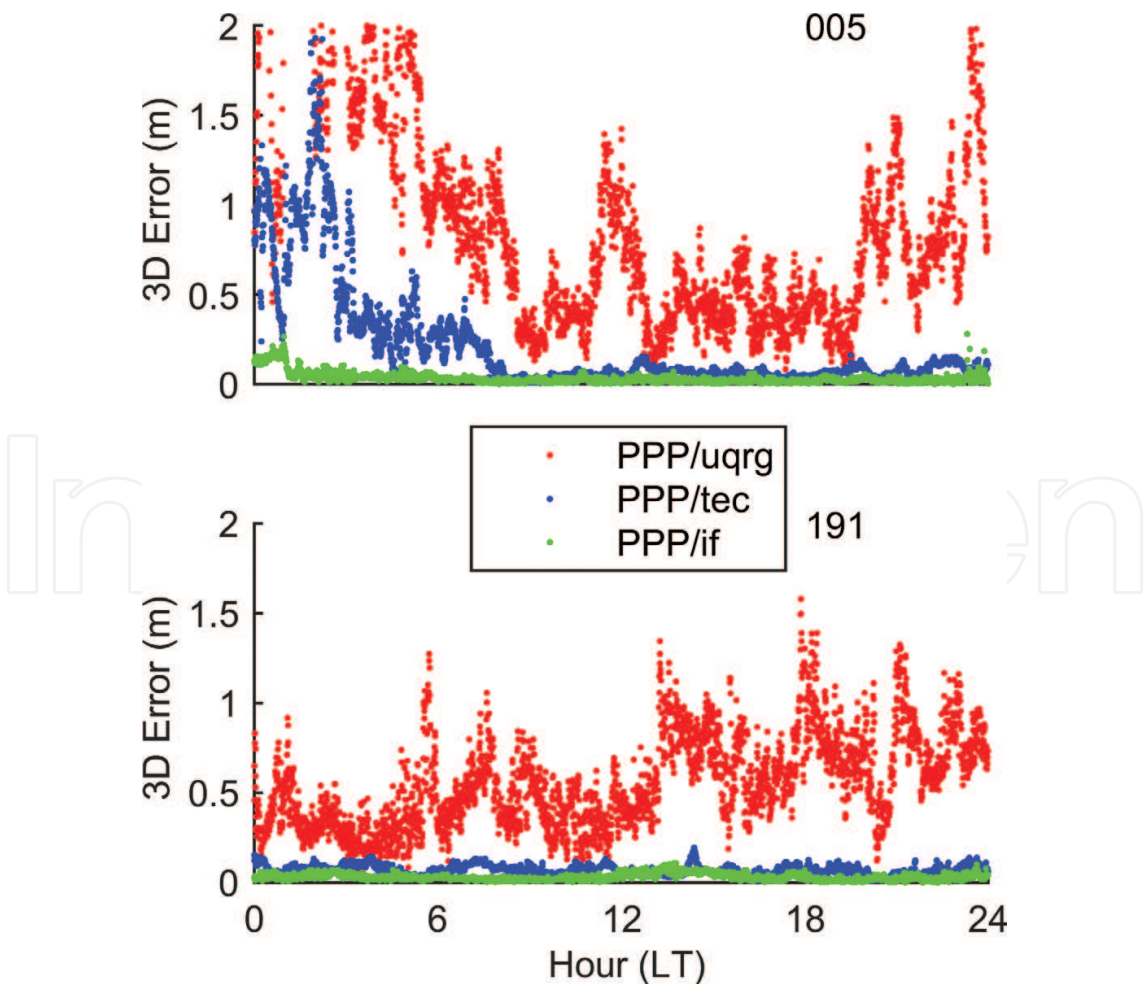

Figure 3. 3D error of PPP at ONRJ station on 2013 for DOY 005 during summer (top panel) and DOY 191 during winter (bottom panel).

was 0.19 m with a standard deviation of 0.05 m and the RMSE of PPP/uqrg was 0.70 m with a standard deviation of 0.66 m. By itself, this is an outstanding result, since many researchers have already used single-frequency receivers and ionospheric corrections to obtain, in general, an absolute accuracy of 0.5 m in the horizontal and 1 m in vertical for the kinematic PPP [96–98]. Now, we are showing the possibility of obtaining the single-frequency PPP accuracy similar to that from dual-frequency PPP. The horizontal accuracy in the experiment for PPP/tec was 0.12 m in DOY 005 and 0.05 m in DOY 191 and the vertical accuracy was 0.15 m in DOY 005 and 0.07 m in DOY 191. These accuracies are compatible to the double-frequency solutions. Therefore, the unique consideration for a high accuracy in single-frequency PPP is that TEC needs to be sufficient precise, which was not realistic in some epochs of DOY 005 due to the ionospheric scintillations.

A noticeable degradation of the PPP solution occurs between 00 and 04 hours LT in the summer solstice due to the high TEC variability. This PPP degradation is related to the ionospheric irregularities that impact GPS observations more effectively. At such instances, the uplifted ionosphere due to the pre-reversal drift produces high vertical gradients. It is believed that these gradients set the preconditions for plasma instability, controlling the generation of ionospheric irregularities. Therefore, the change of the GPS signal phase and amplitude imposed by ionospheric irregularities degrades the PPP solution. It is interesting to note that the PPP/if is sensitive, but not too much, to the ionospheric scintillations. In case of PPP/uqrg, it is hard to see the impact because of the high standard deviation in the PPP solution at other epochs. However, the impact of the scintillations is very evident in PPP/tec. This mainly happens because the estimated TEC was set to be very precise during the PPP, so that TEC was included with small values for standard deviation in the PPP Kalman filter. At epochs where only the first-order ionospheric delay is supposed to affect the GPS observations, the PPP/tec solution is very accurate. At epochs where the high-orders terms of the ionosphere delay impact the GPS signal, the PPP degradation becomes evident.

5. Conclusions

The ionospheric conditions are affected by electrodynamic processes that are driven by solar phenomena. During quiet geomagnetic periods, the effects are clearly associated with the seasonal variation of the solar illumination and with the 11-year solar radiation variation. These conditions can be strongly disturbed under the impact of CMEs (coronal mass ejections) and HSS (high-speed streams) in the magnetosphere producing the geomagnetic storms, which result in steeper electron density gradients and stronger irregularities. These irregularities are responsible for fluctuations in the amplitude and phase of GNSS signals, which can degrade the accuracy of the measurements. Therefore, the climatology of these irregularities is very important to define its spatial distribution and time of occurrence.

The investigation of ionospheric scintillations over South America has shown that they can occur at all longitudinal sectors during quiet geomagnetic periods, but they are stronger at post-sunset hours in the crest regions of the EIA (equatorial ionospheric anomaly), and seems to be more intense in the southern EIA crest, which is under the effect of the SAMA (South American Magnetic Anomaly) [24, 37, 81]. The scintillation occurrences strongly enhance with the increase of the solar activity [20, 21, 35, 37, 99], and during geomagnetic disturbed periods [13, 38, 75, 93, 94].

It was presented the potentiality of a new procedure for TEC calibration, showing a useful tool to correct the first-order ionospheric delay that improves the traditional single-frequency PPP solutions. Additionally, the results show a high-sensitive solution of PPP/tec to the ionospheric scintillations, even more sensitive in comparison with the impact of the ionospheric scintillation in the TEC level, which indicates that this kind of procedures are emerging as having potential for a wide range of applications for those measuring and predicting the ionospheric scintillations.

Acknowledgements

Conflict of interest

The authors declare that they have no conflict of interest.

Author details

Emília Correia[1,2]*, Marcio Tadeu de Assis Honorato Muella[3], Lucilla Alfonsi[4], Fabricio dos Santos Prol[5] and Paulo de Oliveira Camargo[5]

*Address all correspondence to: ecorreia@craam.mackenzie.br

1 National Institute for Space Research - INPE, São José dos Campos, Brazil

2 CRAAM-Presbiterian Mackenzie University, São Paulo, Brazil

3 University of Vale do Paraíba - UNIVAP, São José dos Campos, Brazil

4 National Institute of Geophysics and Vulcanology - INGV, Rome, Italy

5 Universidade Estadual Paulista-UNESP, Presidente Prudente, Brazil

References

[1] Prolss GW. Ionospheric F-region storms. In: Volland H, editor. Handbook of Atmospheric Electrodynamics. Florida: CRC Press; 1995. pp. 195-248

[2] Prolss GW. Ionospheric storms at mid-latitude: A short review. In: Kintner PM Jr, Coster AJ, Fuller-Rowell T, Mannucci AJ, Mendillo M, Heelis R, editors. Midlatitude Ionospheric Dynamics and Disturbances, Geophysical Monograph Series. Vol. 181. Washington, D.C: AGU; 2008. pp. 9-24. DOI: 10.1029/181GM03

[3] Buonsanto MJ. Ionospheric storms – A review. Space Science Reviews. 1999;**88**:563-601. DOI: 10.1023/A:1005107532631

[4] Danilov AD, Lastovicka J. Effects of geomagnetic storms on the ionosphere and atmosphere. International Journal of Geomagnetism and Aeronomy. 2001;**2**(3):209-224

[5] Tsurutani B, Mannucci A, Iijima B, Abdu MA, Sobral JHA, Gonzalez W, Guarnieri F, Tsuda T, Saito A, Yumoto K, Fejer B, Fuller-Rowell TJ, Kozyra J, Foster JC, Coster A, Vasyliunas VM. Global dayside ionospheric uplift and enhancement associated with interplanetary electric fields. Journal of Geophysical Research-Space. 2004;**109**:A08302. DOI: 10.1029/2003JA010342

[6] Yizengaw E, Dyson PL, Essex EA, Moldwin MB. Ionosphere dynamics over the southern hemisphere during the 31 march 2001 severe magnetic storm using multi instrument measurement data. Annales Geophysicae. 2005;**23**:707-721. DOI: 10.5194/angeo-23-707-2005

[7] Mendillo M. Storms in the ionosphere: Patterns and processes for total electron content. Reviews of Geophysics. 2006;**44**:RG4001. DOI: 10.1029/2005RG000193

[8] de Franceschi G, Alfonsi L, Romano V, Aquino MHO, Dodson A, Mitchell CN, Wernik AW. Dynamics of high latitude patches and associated small scale irregularities. Journal of Atmospheric and Solar - Terrestrial Physics. 2008;**70**:879-888. DOI: 10.1016/j.jastp.2007.05.018

[9] Danilov AD. Ionospheric F-region response to geomagnetic disturbances. Advances in Space Research. 2013;**52**:343-366. DOI: 10.1016/j.asr.2013.04.019

[10] Thomas EG, Baker JBH, Ruohoniemi JM, Clausen LBN, Coster AJ, Foster JC, Erickson PJ. Direct observations of the role of convection electric field in the formation of a polar tongue of ionization from storm enhanced density. Journal of Geophysical Research-Space. 2013;**118**:1180-1189. DOI: 10.1002/jgra.50116

[11] Horvath I, Lovell BC. Storm-enhanced plasma density and polar tongue of ionization development during the 15 May 2005 super storm. Journal of Geophysical Research-Space. 2015;**120**:5101-5116. DOI: 10.1002/2014JA020980

[12] Prikryl P, Ghoddousi-Fard R, Weygand JM, Viljanen A, Connors M, Danskin DW, Jayachandran PT, Jacobsen KS, Andalsvik YL, Thomas EG, Ruohoniemi JM, Durgonics T, Oksavik K, Zhang Y, Spanswick E, Aquino M, Sreeja V. GPS phase scintillation at high latitudes during the geomagnetic storm of 17-18 March 2015. Journal of Geophysical Research-Space. 2016;**121**:10448-10465. DOI: 10.1002/2016JA023171

[13] Correia E, Spogli L, Alfonsi L, Cesaroni C, Gulisano AM, Thomas EG, Ramirez RFH, Rodel AA. Ionospheric F-region response to the 26 September 2011 geomagnetic storm in the Antarctica American and Australian sectors. Annales Geophysicae. 2017;**35**:1113-1129. DOI: 10.5194/angeo-35-1113-2017

[14] Conker RS, El-Arini B, Hegarty CJ, Hsiao T. Modeling the effects of ionospheric scintillation on GPS/satellite-based augmentation system availability. Radio Science. 2003;**38**(1). DOI: 1001. DOI: 10.1029/2000RS002604

[15] Xu R, Liu Z, Li M, Morton Y, Chen W. An analysis of low latitude ionospheric scintillation and its effects on precise point positioning. Journal of Global Positioning Systems. 2012;**11**:22-32. DOI: 10.5081/jgps.11.1.22

[16] Marques HAS, Monico JFG, Marques HA. Performance of the L2C civil GPS signal under various ionospheric scintillation effects. GPS Solutions. 2016;**20**:139-149. DOI: 10.1007/s10291-015-0472-2

[17] Aquino M, Andreotti M, Dodson AH, Strangeways H. On the use of ionospheric scintillation indices as input to receiver tracking models. Advances in Space Research. 2007;**40**:426-435. DOI: 10.1016/j.asr.2007.05.035

[18] Kintner PM, Ledvina BM, de Paula ER. GPS and ionospheric scintillations. Space Weather. 2007;**5**:S09003. DOI: 10.1029/2006SW000260

[19] Spogli L, Alfonsi L, De Franceschi G, Romano V, Aquino MHO, Dodson A. Climatology of GPS ionospheric scintillations over high and mid-latitude European regions. Annales Geophysicae. 2009;**27**:3429-3437. DOI: 10.5194/angeo-27-3429-2009

[20] Aarons J. Global morphology of ionospheric scintillation. Proceedings of the IEEE. 1982;**70**:360-378. DOI: 10.1109/PROC.1982.12314

[21] Sobral JHA, Abdu MA, Takahashi H, Taylor MJ, de Paula ER, Zamlutti CJ, Aquino MG, Borba GL. Ionospheric plasma bubble climatology over Brazil based on 22 years (1977-1998) of 630 nm airglow observations. Journal of Atmospheric and Terrestrial Physics. 2002;**64**:1517-1524. DOI: 10.1016/S1364-6826(02)00089-5

[22] Abdu MA, Kherani EA, Batista IS, de Paula ER, Fritts DC, Sobral JHA. Gravity wave initiation of equatorial spread F/plasma bubble irregularities based on observational data from the Spread FEx campaign. Annales Geophysicae. 2009;**27**:2607-2622. DOI: 10.5194/angeo-27-2607-2009

[23] Cabrera MA, Pezzopane M, Zuccheretti E, Ezquer RG. Satellite traces, range spread-F occurrence, and gravity wave propagation at the southern anomaly crest. Annales Geophysicae. 2010;**28**:1133-1140. DOI: 10.5194/angeo-28-1133-2010

[24] Spogli L, Alfonsi L, Cilliers PJ, Correia E, De Franceschi G, Mitchell CN, Romano V, Kinrade J, Cabrera MA. GPS scintillations and total electron content climatology in the southern low, middle and high latitude region. Annals of Geophysics. 2013;**56**:R0220. DOI: 10.4401/ag-6240

[25] Li G, Ning B, Ren Z, Hu L. Statistics of GPS ionospheric scintillation and irregularities over polar regions at solar minimum. GPS Solutions. 2010;**14**:331-341. DOI: 10.1007/s10291-009-0156-x

[26] Alfonsi L, Spogli L, De Franceschi G, Romano V, Aquino M, Dodson A, Mitchell CN. Bipolar climatology of GPS ionospheric scintillation at solar minimum. Radio Science. 2011;**46**. DOI: RS0D05.DOI: 10.1029/2010RS004571

[27] Chatterjee S, Chakraborty SK. Variability of ionospheric scintillation near the equatorial anomaly crest of the Indian zone. Annales Geophysicae. 2013;**31**:697-711. DOI: 10.5194/angeo-31-697-2013

[28] Bhattacharyya A, Kakad B, Sripathi S, Jeeva K, Nair KU. Development of intermediate scale structure near the peak of the F region within an equatorial plasma bubble. Journal of Geophysical Research. 2014;**119**:3066-3076. DOI: 10.1002/2013JA019619

[29] Akala AO, Amaeshi LLN, Somoye EO, Idolor RO, Okoro E, Doherty PH, Groves KM, Carrano CS, BridgwoodC T, Baki P, D'ujanga FM, Seemala GK. Climatology of GPS amplitude scintillations over equatorial Africa during the minimum and ascending phases of solar cycle 24. Astrophys Space Science. 2015;**357**:17. DOI: 10.1007/s10509-015-2292-9

[30] Cesaroni C, Spogli L, Alfonsi L, de Franceschi G, Ciraolo L, JFG M, Scotto C, Romano V, Aquino M, Bougard B. L-band scintillations and calibrated total electron content gradients over Brazil during the last solar maximum. Journal Space Weather and Space Climate. 2015;**5**:A36. DOI: 10.1051/swsc/2015038

[31] Zhang H, Liu Y, Wu J, Xu T, Sheng D. Observations and modeling of UHF-band scintillation occurrence probability over the low-latitude region of China during the maximum activity of solar cycle 24. Annales Geophysicae. 2015;**33**:93-100. DOI: 10.5194/angeo-33-93-2015

[32] Srinivasu VKD, Brahmanandam PS, Uma G, Prasad DSVVD, Rao PVSR, Mukherjee S. Long-term morphological and power spectral studies of VHF amplitude scintillations recorded over Waltair (17.7_ N, 83.3_ E), India. Terrestrial, Atmospheric and Oceanic Sciences. 2016;**28**:385-394. DOI: 10.3319/TAO.2016.11.08.01

[33] Moraes AO, Costa E, Abdu MA, Rodrigues FS, de Paula ER, Oliveira K, Perrela WJ. The variability of low-latitude ionospheric amplitude and phase scintillation detected by a triple-frequency GPS receiver. Radio Science. 2017;**52**:439-460. DOI: 10.1002/2016RS006165

[34] Muella MTAH, de Paula ER, Monteiro AA. Ionospheric scintillation and dynamics of Fresnel-scale irregularities in the inner region of the equatorial ionization anomaly. Surveys in Geophysics. 2013;**34**:233-251. DOI: 10.1007/s10712-012-9212-0

[35] Muella MTAH, de Paula ER, Jonah OF. GPS L1-frequency observations of equatorial scintillations and irregularity zonal velocities. Surveys in Geophysics. 2014;**35**:335-357. DOI: 10.1007/s10712-013-9252-0

[36] Marques HA, Marques HAS, Aquino M, Sreeja VV, Monico JFG. Accuracy assessment of precise point positioning with multi-constellation GNSS data under ionospheric scintillation effects. Journal of Space Weather and Space Climatology. 2018;**8**:A15. DOI: 10.1051/swsc/2017043

[37] Muella MTAH, Duarte-Silva MH, Moraes AO, de Paula ER, de Rezende LFC, Alfonsi L, Affonso BJ. Climatology and modeling of ionospheric scintillations and irregularity zonal drifts at the equatorial anomaly crest region. Annales Geophysicae. 2017;**35**:1201-1218. DOI: 10.5194/angeo-35-1201-2017

[38] de Paula ER, Kherani EA, Abdu MA, Batista IS, SobralJ HA, Kantor IJ, Takahashi H, Rezende LFC, Muella MTAH, Rodrigues FS, Kintner PM, LedvinaB M, Mitchell C, Groves KM. Characteristics of the ionospheric irregularities over Brazilian longitudinal sector. Indian Journal of Radio & Space Physics. 2007;**36**:268-277

[39] Akala AO, Doherty PH, Valladares CE, Carrano CS, Sheehan R. Statistics of GPS scintillations over South America at three levels of solar activity. Radio Science. 2011;**46**:RS5018. DOI: 10.1029/2011RS004678

[40] Spogli L, Alfonsi L, Romano V, Franceschi GD, Monico JFG, Shimabukuro MH, Bourgard B, Aquino M. Assessing the GNSS scintillation climate over Brazil under increasing solar activity. Journal of Atmospheric and Terrestrial Physics. 2013;**105**:199-206. DOI: 10.1016/j.jastp.2013.10.003

[41] Forbes JM, Bruinsma SL, Zhang X, Oberheide J. Surface-exosphere coupling due to thermal tides. Geophysical Research Letters. 2009;**36**:L15812. DOI: 10.1029/2009GL038748

[42] Fuller-Rowell TJ, Codrescu MV, Moffett RJ, Quegan S. Response of the thermosphere and ionosphere to geomagnetic storms. Journal of Geophysical Research. 1994;**99**(A3):3893-3914. DOI: 10.1029/93JA02015

[43] Richmond AD. The ionospheric wind dynamo: Effects of its coupling with different atmospheric regions, in the upper mesosphere and lower thermosphere: A review of experiment and theory. In: Johnson RM, Killeen TL, editors. Geophysical Monograph Series. Vol. 87. Washington, D.C: AGU; 1995. pp. 49-65. DOI: 10.1029/GM087p0049

[44] Heelis RA. Electrodynamics in the low and middle latitude ionosphere: A tutorial. Journal of Atmospheric and Solar - Terrestrial Physics. 2004;**66**:825-838. DOI: 10.1016/j.jastp.2004.01.034

[45] Fejer BG. Low latitude ionospheric electrodynamics. Space Science Reviews. 2011;**158**:145-166. DOI: 10.1007/s11214-010-9690-7

[46] Richmond AD. Ionospheric electrodynamics. In: Volland H, editor. Handbook of Atmospheric Electrodynamics. Florida: CRC Press; 1995. pp. 249-290

[47] Fejer BG. The electrodynamics of the low-latitude ionosphere: Recent results and future challenges. Journal of Atmospheric and Solar - Terrestrial Physics. 1997;**59**:1465-1482. DOI: 10.1016/S1364-6826(96)00149-6

[48] Namba S, Maeda K-I. Radio Wave Propagation. Vol. 86. Tokyo: Corona; 1939

[49] Pancheva D, Apostolov E, Lastovicka J, Boska J. Long-period fluctuations of meteorological origin observed in the lower ionosphere. Journal of Atmospheric and Solar - Terrestrial Physics. 1989;**51**:381-388. DOI: 10.1016/0021-9169(89)90120-7

[50] Chen P-R. Two-day oscillation of the equatorial ionization anomaly. Journal of Geophysical Research. 1992;**97**(A5):6343-6357. DOI: 10.1029/91JA02445

[51] Forbes JM, Leveroni S. Quasi 16-day oscillation in the ionosphere. Geophysical Research Letters. 1992;**19**(10):981-984. DOI: 10.1029/92GL00399

[52] Parish HF, Forbes JM, Kamalabadi F. Planetary wave and solar emission signatures in the equatorial electrojet. Journal of Geophysical Research. 1994;**99**(A1):355-368. DOI: 10.1029/93JA02096

[53] Lastovicka J, Ebel A, Ondraskova A. On the transformation of planetary waves of tropospheric origin into waves in radio wave absorption in the lower ionosphere. Studia Geophysica et Geodaetica. 1994;**38**:71-81. DOI: 10.1007/BF02296254

[54] Immel TJ, Mende SB, Hagan ME, KintnerP M, England SL. Evidence of tropospheric effects on the ionosphere. Eos. 2009;**90**:69-80. DOI: 10.1029/2009EO090001

[55] Correia E, Raulin J-P, Kaufmann P, Bertoni F, Quevedo MT. Inter-hemispheric analysis of daytime low ionosphere behavior from 2007 to 2011. Journal of Atmospheric and Solar - Terrestrial Physics. 2013;**92**:51-58. DOI: 10.1016/j.jastp.2012.09.006

[56] Woodman RF, La Hoz C. Radar observations of F-region equatorial irregularities. Journal of Geophysical Research. 1976;**81**:5447-5466. DOI: 10.1029/JA081i031p05447

[57] Woodman R. Vertical drift velocities and east-west electric fields at the magnetic equator. Journal of Geophysical Research. 1970;**75**(31):6249-6259. DOI: 10.1029/JA075i031p06249

[58] Fejer BG. Low latitude electrodynamics plasma drifts: A review. Journal of Atmospheric and Solar - Terrestrial Physics. 1991;**53**:677-693. DOI: 10.1016/0021-9169(91)90121-M

[59] Kelley MC. The Earth's Ionosphere. London: Academic Press; 1989. p. 580

[60] Abdu MA, de Medeiros RT, Sobral JHA, Bittencourt JA. Spread F plasma bubble vertical rise velocities determined from spaced ionosonde observations. Journal of Geophysical Research. 1983;**88**:9197-9204. DOI: 10.1029/JA088iA11p09197

[61] Valladares CE, Villalobos J, Sheehan R, Hagan MP. Latitudinal extension of low-latitude scintillations measured with a network of GPS receivers. Annales Geophysicae. 2004;**22**:3155-3175. DOI: 10.5194/angeo-22-3155-2004

[62] Gwal AK, Dubey S, Wahi R. A study of L-band scintillations at equatorial latitudes. Advances in Space Research. 2004;**34**:2092-2095. DOI: 10.1016/j.asr.2004.08.005

[63] Abdu MA, Sobral JHA, BastitaI S, Rios VH, Medina C. Equatorial spread-F occurrence statistics in the American longitudes: Diurnal, seasonal and solar cycle variations. Advances in Space Research. 1998;**22**:851-854. DOI: 10.1016/S0273-1177(98)00111-2

[64] Abdu MA, SobralJ HA, BatistaI S. Equatorial spread-F statistics in the American longitudes: Some problems relevant to ESF description in the IRI scheme. Advances in Space Research. 2000;**25**:113-124. DOI: 10.1016/S0273-1177(99)00907-2

[65] Sastri JH. Equatorial electric fields of the disturbance dynamo origin. Annales Geophysicae. 1988;**6**:635-642

[66] Tsurutani BT, Verkhoglyadova OP, Mannucci AJ, Saito A, Araki T, Yumoto K, Tsuda T, Abdu MA, Sobral JHA, Gonzalez WD, McCreadie H, Lakhina GS, Vasyliunas VM. Prompt penetration electric fields (PPEFs) and their ionospheric effects during the

great magnetic storm of 30-31 October 2003. Journal of Geophysical Research-Space. 2008;**113**:A05311. DOI: 10.1029/2007JA012879

[67] Huang C-S, Foster JC, Kelley MC. Long duration penetration of the interplanetary electric field to the low-latitude ionosphere during the main phase of magnetic storms. Journal of Geophysical Research-Space. 2005;**110**:A11309. DOI: 10.1029/2005JA011202

[68] Mannucci AJ, Tsurutani BT, Abdu MA, Gonzalez WD, Komjathy A, Echer E, Iijima BA, Crowley G, Anderson D. Superposed epoch analysis of the dayside ionospheric response to four intense geomagnetic storms. Journal of Geophysical Research-Space. 2008;**113**:A00A02. DOI: 10.1029/2007JA012732

[69] Gonzalez WD, Joselyn JA, Kamide Y, Kroehl HW, Rostoker G, Tsurutani BT, Vasyliunas VM. What is a geomagnetic storm? Journal of Geophysical Research-Space. 1994;**99**:5771-5792. DOI: 10.1029/93JA02867

[70] Yeh KC, Liu CH. Radio-wave scintillations in the ionosphere. Proceedings of IEEE. 1982;**70**:324-360. DOI: 10.1109/PROC.1982.12313

[71] Van Dierendonck AJ, Klobuchar J, Hua Q. Ionospheric scintillation monitoring using commercial single frequency C/A code receivers. In: Proceedings of the Sixth International Technical Meeting of the Satellite Division of the Institute of Navigation (ION GPS-93); 22-24 September 1993. Salt Lake City: ION GPS; 1993. pp. 1333-1342

[72] Basu S, Groves KM. Specification and forecasting of outages on satellite communication and navigation systems. Space Weather, Geophysical Monograph, American Geophysical Union, Washington, DC. 2001;**125**:424-430. DOI: 10.1029/GM125p0423

[73] Abdu MA, Bittencourt JA, Batista IS. Magnetic declination of the equatorial F-region dynamo electric field development and spread F. Journal of Geophysical Research. 1981;**86**(467):11443-11446. DOI: 10.1029/JA086iA13p11443

[74] Batista I, Abdu M, Bittencourt J. Equatorial F region vertical plasma drifts: Seasonal and longitudinal asymmetries in the American sector. Journal of Geophysical Research-Space. 1986;**91**:12055-12064. DOI: 10.1029/JA091iA11p12055

[75] Abdu MA, Batista IS, Carrasco AJ, Brum CGM. South Atlantic magnetic anomaly ionization: A review and a new focus on electrodynamic effects in the equatorial ionosphere. Journal of Atmospheric and Solar - Terrestrial Physics. 2005;**67**:1643-1657. DOI: 10.1016/j.jastp.2005.01.014

[76] Valladares CE, Chau JL. The low-latitude ionosphere sensor network: Initial results. Radio Science. 2012;**47**:RS0L17. DOI: 10.1029/2011RS004978

[77] Vani BC, Shimaburo MH, Monico JFG. Visual exploration and analysis of ionospheric scintillation monitoring data: The ISMR query tool. Computers and Geosciences. 2016;**104**:125-134. DOI: 10.1016/j.cageo.2016.08.022

[78] Fejer BG, de Paula ER, Gonzalez SA, Woodman RF. Average vertical and zonal F region plasma drifts over Jicamarca. Journal of Geophysical Research. 1991;**96**:13901-13906. DOI: 10.1029/91JA01171

[79] Sousasantos J, de Oliveira Moraes A, Sobral JHA, Muella MTAH, de Paula ER, Paolini RS. Climatology of the scintillation onset over southern Brazil. Annales Geophysicae. 2018;**36**:565-576. DOI: 10.5194/angeo-36-565-2018

[80] Basu S, Kudeki E, Basu S, Valladares CE, Weber EJ, Zengingonul HP, Bhattacharyya S, Sheehan R, Meriwether JW, Biondi MA, Kuenzler H, Espinoza J. Scintillations, plasma drifts, and neutral winds in the equatorial ionosphere after sunset. Journal of Geophysical Research. 1996;**101**:26795-26809. DOI: 10.1029/96JA00760

[81] de Paula ER, Muella MTAH, Sobral JHA, Abdu MA, Batista IS, Beach TL, Groves KM. Magnetic conjugate point observations of kilometer and hundred-meter scale irregularities and zonal drifts. Journal of Geophysical Research. 2010;**115**:A08307. DOI: 10.1029/2010JA015383

[82] Valladares CE, Meriwether JW, Sheehan R, Biondi MA. Correlative study of neutral winds and scintillation drifts measured near the magnetic equator. Journal of Geophysical Research. 2002;**107**. DOI: SIA7. DOI: 10.1029/2001JA000042

[83] Kil H, Kintner PM, de Paula ER, Kantor IJ. Latitudinal variations of scintillation activity and zonal plasma drifts in South America. Radio Science. 2002;**37**:1006. DOI: 10.1029/2001RS002468

[84] Engavale B, Jeeva K, Nair KU, Bhattacharyya A. Solar flux dependence of coherence scales in scintillation patterns produced by ESF irregularities. Annales Geophysicae. 2005;**23**:3261-3266. DOI: 10.5194/angeo-23-3261-2005

[85] Fejer BG, Souza JR, Santos AS, Pereira AEC. Climatology of F region zonal plasma drifts over Jicamarca. Journal of Geophysical Research. 2005;**110**:A12310. DOI: 10.1029/2005JA011324

[86] Sobral JHA, Abdu MA, Pedersen TR, Castilho VM, Arruda DCS, Muella MTAH, Batista IS, Mascarenhas M, de Paula ER, Kintner PM, Kherani EA, Medeiros AF, Buriti RA, Takahashi H, Schuch NJ, Denardini CM, Zamlutti CJ, Pimenta AA, Souza JR, Bertoni FCP. Ionospheric zonal velocities at conjugate points over Brazil during the COPEX campaign: Experimental observations and theoretical validations. Journal of Geophysical Research. 2009;**114**:A04309. DOI: 10.1029/2008JA013896

[87] Seaton MJ. A possible explanation of the drop in F-region critical densities accompanying many ionospheric storms. Journal of Atmospheric and Terrestrial Physics. 1956;**8**:122-124. DOI: 10.1016/0021-9169(56)90102-7

[88] Prolss GW, Jung MJ. Travelling atmospheric disturbances as a possible explanation for daytime positive storm effects of moderate duration at middle latitudes. Journal of Atmospheric and Terrestrial Physics. 1978;**40**:1351-1354. DOI: 10.1016/0021-9169(78)90088-0

[89] Foster JC. Ionospheric-magnetospheric-heliospheric coupling: Storm-time thermal plasma redistribution. In: Kintner PM, Coster AJ, Fuller-Rowell T, Mannucci AJ, Mendillo M, Heelis R, editors. Mid-Latitude Dynamics and Disturbances. Geophysical Monograph Series. Vol. 181. 2008. pp. 121-134. DOI: 10.1029/181GM12

[90] Sandel BR, King RA, Forrester WT, Gallagher DL, Broadfoot AL, Curtis CC. Initial results from the IMAGE extreme ultraviolet imager. Geophysical Research Letters. 2001;**28**:1439-1442. DOI: 10.1029/2001GL012885

[91] Skone S, Man F, Ghafoori F, Tiwari R. Investigation of scintillation characteristics for high latitude phenomena. Proceedings of the ION GNSS 2008. 2008;**SessionD5**:2425-2434

[92] Kinrade J, Mitchell CN, Smith ND, Ebihara Y, Weatherwax AT, Bust GS. GPS phase scintillation associated with optical auroral emissions: First statistical results from the geographic south pole. Journal of Geophysical Research-Space. 2013;**118**:2490-2502. DOI: 10.1002/jgra.50214

[93] de Abreu AJ, Fagundes PR, Gende M, Bolaji OS, de Jesus R, Brunini C. Investigation of ionospheric response to two moderate geomagnetic storms using GPS–TEC measurements in the south American and African sectors during the ascending phase of solar cycle 24. Advances in Space Research. 2014;**53**:1313-1328. DOI: 10.1016/j.asr.2014.02.011

[94] de Abreu AJ, Martin IM, Fagundes PR, Venkatesh K, Batista IS, de Jesus R, Rockenback M, Coster A, Gende M, Alves MA, Wild M. Ionospheric F-region observations over American sector during an intense space weather event using multi-instruments. Journal of Atmospheric and Solar - Terrestrial Physics. 2017;**156**:1-14. DOI: 10.1016/j.jastp.2017.02.009

[95] Prol FS, Camargo PO, Monico JFG, Muella MTAH. Assessment of a TEC calibration procedure by single frequency PPP. GPS Solutions. 2018;**22**:35. DOI: 10.1007/s10291-018-0701-6

[96] Ø-vstedal O. Absolute positioning with single-frequency GPS receivers. GPS Solutions. 2002;**5**:33-44

[97] Le AQ, Tiberius C. Single-frequency precise point positioning with optimal filtering. GPS Solutions. 2007;**11**:61-69

[98] Sterle O, Stopar B, Prešeren PP. Single-frequency precise point positioning: An analytical approach. Journal of Geodesy. 2015;**89**:793-810

[99] Sreeja VV, Aquino M, Forte B, Elmas Z, Hancock C, de Franceschi G, Alfonsi L, Spogli L, Romano V, Bougard B, Monico JFG, Wernik AW, Sleewaegen J-M, Canto A, da Silva EF. Tackling ionospheric scintillation threat to GNSS in Latin America. Journal of Space Weather and Space Climate. 2011;**1**:A05. DOI: 10.1051/swsc/2011005